PHYSICAL REVIEW B VOLUME 52, NUMBER 22 1 DECEMBER 1995-II

sp^3 content of mass-selected ion-beam-deposited carbon films determined by inelastic and elastic electron scattering

J. Kulik
Texas Center for Superconductivity, University of Houston, Houston, Texas 77204

G. D. Lempert and E. Grossman
Soreq Nuclear Research Center, Yavne 81800, Israel

D. Marton and J. W. Rabalais
Department of Chemistry, University of Houston, Houston, Texas, 77204

Y. Lifshitz
Soreq Nuclear Research Center, Yavne 81800, Israel
(Received 28 June 1995; revised manuscript received 31 August 1995)

Amorphous carbon films grown by low-energy mass-selected ion-beam deposition have been characterized by inelastic and elastic electron scattering. Films were grown using deposition energies from 10 up to 2000 eV. Most samples were deposited at room temperature with a few deposited at elevated substrate temperatures. Transmission electron-energy-loss spectra were recorded for all films both in the low-energy-loss region, where the bulk plasmon excitation is the primary feature of interest, and in the vicinity of the carbon K edge where the data were used to estimate the fraction of sp^3 bonded atoms. Elastic-electron-scattering data were also recorded, and bond lengths and angles were extracted from these data. The carbon K-edge spectra indicate that the highest sp^3 content (about 80%) occurs for films grown with ion beam energies between about 50 and 600 eV and, furthermore, that the sp^3 content remains greater than 50% for deposition energies up to 2000 eV. Bond lengths and angles extracted from elastic-electron-scattering data support the conclusions drawn from the energy-loss data.

INTRODUCTION

There has recently been significant interest in the use of low-energy (1–1000 eV) ion or atom species for the growth of thin films.[1–8] Films grown by this method often exhibit unusual and desirable properties. Carbon, for example, is of particular interest because the use of hyperthermal energies for the carbon atoms or ions can result in films with diamondlike properties as demonstrated by Aisenberg and Chabot.[9] Apparently, growth processes arising from the use of hyperthermal species result in the characteristics of these films. Indeed, *in situ* monitoring of film characteristics during growth had led Lifshitz and co-workers to propose a "subplantation" model to describe film evolution.[10,11] According to this model, film growth proceeds as a result of a shallow implantation process. Collisional stopping processes and incorporation of impinging species into subsurface layers govern the evolution of the film. Such subsurface processes undoubtedly give rise to large internal stresses in the growing film. In fact, some investigators have approached the problem of understanding the growth and properties of these films by emphasizing the role of such stresses.[12–15] This has further led to the development of quantitative models to explain the formation of compressive stress in films deposited with bombardment of energetic ions or atoms.[16,17]

The diamondlike carbon (DLC) samples grown using hyperthermal carbon species, although amorphous, are extremely hard, chemically inert, and electrically insulating. Of fundamental interest is the nature of the chemical bonding in these films. There is abundant evidence[12–15,18–24] to support the conclusion that those films exhibiting diamondlike properties, e.g., high hardness and resistivity, contain high concentrations (up to about 80%) of sp^3 hybridized carbon atoms. Much of this evidence consists of electron-energy-loss spectroscopy (EELS),[12–15,18–21] both in the low-energy-loss range where the bulk plasmon excitation is present and in the higher-energy-loss range at the carbon K edge. There is also structural evidence, both from neutron diffraction[22,23] and from energy filtered electron diffraction,[12–14,24] that the bond lengths and angles more closely resemble those of diamond than those of graphite. Preliminary investigations using high-resolution transmission electron microscopy (TEM) have also confirmed that the structure of these films is intrinsically different from that of evaporated amorphous carbon.[25]

Researchers have investigated a variety of different methods of growing carbon films with the resulting samples varying in their degree of diamondlike properties.[3,7] There are, of course, a number of different parameters in the deposition process which determine the final film properties; for many of the growth methods the intrinsic deposition parameters are difficult to define and control. This may explain a number of inconsistencies in the literature. For example, there are at present contradictory data on the effect of ion-beam energy on the final film properties. Optimal energy ranges reported by different investigators vary from a relatively low and narrow window of 20–40 eV determined by McKenzie and co-workers[12,14] to a higher and much broader window of 100–700 eV determined by Hirvonen *et al.*[26] Others have

0163-1829/95/52(22)/15812(11)/$06.00 © 1995 The American Physical Society

reported still different optimal windows.[15,27]

The film preparation method that we have employed is mass-selected ion-beam deposition (MSIBD). This method, which has now been used by several different groups to study the growth of DLC films,[26–33] is unique among the various deposition methods in its ability to control the physical parameters relevant to film growth and properties.[4,34]

In this paper we are concerned primarily with the effect of the energy of the impinging ions in determining the degree of sp^3 bonding. We present spectroscopic data from carbon films deposited over a wide range of ion beam energies from 10 up to 2000 eV. For each energy studied, one or more depositions were performed at ambient substrate temperatures, and, for some energies, depositions were done at elevated temperatures. In addition to the spectroscopic data, we also present structural data for the ambient temperature depositions. Our results help to clarify the role of ion energy in the film growth process and, furthermore, may aid in the refinement of existing growth models[16,17] or the development of new ones.

Our spectroscopic data are from EELS measurements. These spectra were recorded using transmission geometry, so they are sensitive to bulk properties. It is well known that spectral fine structure in the vicinity of core ionization edges is a potentially powerful tool for the study of atomic coordination and bonding in solids.[35] Fine structure at the carbon K edge has been qualitatively employed by a number of researchers for the determination of the sp^3 content in amorphous carbon films.[15,18,19,21] In this paper, which is an extension of a previous study[21] concerning the narrower deposition energy range of 50 to 300 eV, we present detailed information on our own EELS studies both at the carbon K edge and in the low loss region of the spectrum where we have measured the bulk plasmon energies. These data, in preliminary form, comprised part of an earlier study on these and other films using a host of characterization techniques.[36–38] Our data show that there is an optimum ion energy range of about 50 to 600 eV for the formation of films which are predominantly sp^3 bonded. Of further significance is the fact that the sp^3 fraction remains above 50% for ion beam energies up to 2000 eV. Values for the plasmon resonance energies, presumably indicative of film densities, correlate well with the degree of diamondlike (sp^3) bonding.

Our structural data are obtained using energy filtered electron diffraction. Bond lengths extracted from the diffraction data support the interpretation of the K-edge spectra in terms of the degree of sp^3 bonding. We also discuss several difficulties which arise in interpreting energy filtered electron diffraction from carbon samples.

EXPERIMENT

A. Film growth

The carbon films were grown with the low-energy MSIBD technique using the facilities at Soreq NRC which have been described elsewhere.[39] Deposition energies used were 10, 20, 30, 50, 120, 300, 600, 990, and 2000 eV. The peak deposition rate was about 8×10^{14} atoms/s cm^2 for 10 eV ions. The rate increases to 6×10^{15} atoms/s cm^2 for 120 eV ions and is about 10^{16} atoms/s cm^2 for ion energies above 300 eV. The average deposition rates were about an order of magnitude lower than these values because of mechanical scanning used to achieve large (>1 cm$\times1$ cm), homogeneous samples. The relatively high deposition rates achievable at Soreq are possible because of the large current densities available—as much as a thousand times greater than the highest current densities used in the original MSIBD work at Houston.[32] The energy distribution width of the ion beam was 5 eV independent of the energy (compared with 3 eV at Houston). Substrates were ambient temperature Si (100) wafers. In addition to this systematic study of deposition energies, we also performed a qualitative study of the effect of substrate temperature; depositions at 120 eV were performed at temperatures of 130 and 205 °C, and a 300 eV deposition was done at 165 °C. Film thicknesses were measured by optical interference and by profilometry.

B. Electron-energy-loss spectroscopy and quantitative diffraction

Preparation of samples for the transmission electron microscope and experimental parameters for EELS acquisition are described elsewhere.[21] For each of the films, we recorded energy-loss spectra in the vicinity of the carbon K edge at about 285 eV. The background was removed using established procedures.[40] For each K-edge spectrum recorded, we also recorded a low-energy-loss spectrum from 0 up to about 160 eV loss. From these spectra we determined the plasmon resonance energy for each film. Availability of the low-loss spectrum also allows the single scattering distribution for the K-edge spectra to be approximately recovered by standard deconvolution procedures.[40] As the films range in thickness from about 34 up to about 110 nm, extraction of single scattering distributions facilitates comparison among different spectra.

It is known that the scintillator-photodiode array combination used to detect the electrons in the Gatan Model 666 spectrometer has a single channel response function that deviates significantly from the desired delta function.[41] All spectra which we have recorded have been deconvolved with the zero loss beam profile to compensate for this instrumental effect.

We have also recorded quantitative diffraction data by using the spectrometer as an energy filter to select the elastically scattered signal as a function of angle. We used a 200 keV primary beam, and the angular resolution was 0.25 mrad. The scattering vector was calibrated using a film of evaporated polycrystalline gold inserted in the sample chamber together with the carbon films.

RESULTS

A. Energy-loss spectroscopy

1. Room-temperature depositions

Typical single scattering distributions extracted from K-edge spectra are shown in Fig. 1 for samples grown using deposition energies of 10, 120, and 2000 eV at ambient temperature. Common features include a peak at about 285 eV and a second, broader peak at about 295 eV. The first peak is commonly attributed to π^* antibonding states while the second is attributed to σ^* antibonding states. The inset in Fig. 1, showing the K edge from the 120 eV film, is a comparison of

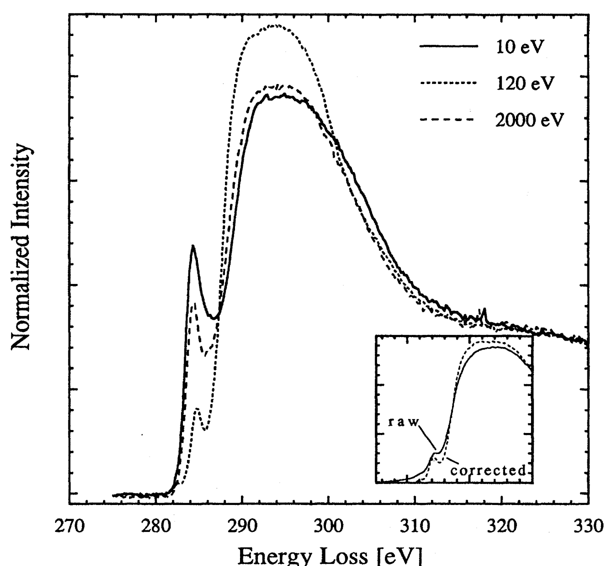

FIG. 1. Energy-loss spectra at the carbon K edge for three samples of MSIBD amorphous carbon films. The π^* feature at about 285 eV is observed to be weakest within a deposition energy window between about 50 and 600 eV. The inset shows the effect of correcting for the imperfect detector response.

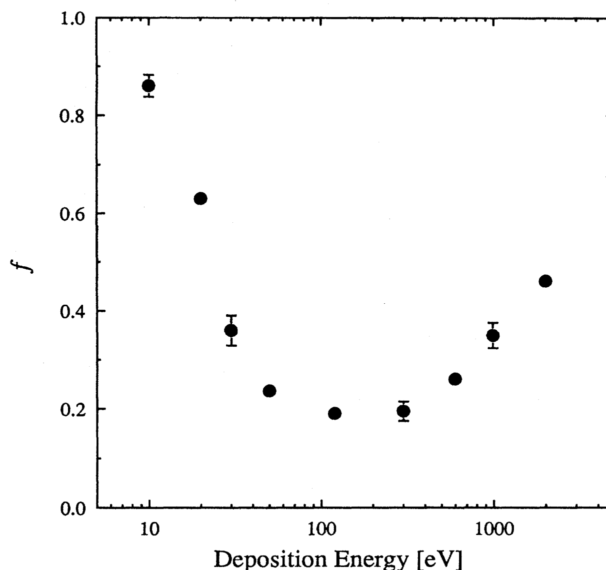

FIG. 2. Plot of normalized integral of π^* peak vs deposition energy showing a broad minimum between about 50 and 600 eV.

raw data (background subtracted) from the detector with data corrected for the detector response.[41]

A proper normalization of the data which allows valid comparison among films with different K-edge spectral structure is not obvious. An ideal experiment would employ films of equal mass thickness and a primary electron beam with a fixed intensity reproducible from one measurement to the next. This procedure would then also avoid the problem of extracting single scattering distributions. Since such an ideal experiment is not possible, we have chosen to extract the single scattering and to normalize these spectra by equating the number of counts in a relatively large energy window starting at the edge onset.[21] This method, clearly somewhat arbitrary, is essentially the same as that used by Berger, McKenzie, and Martin.[18] This normalization could conceivably affect the strengths of the spectral features at the ionization edge, especially the σ^* peak which contains significant intensity, thereby causing uncertainty in comparisons among spectra from different samples. An alternative method would be to employ a small normalization window at a high energy loss far from the onset. However, we emphasize that in the first method, if the normalization window is large enough, the result will approach that of the second method. Our window is sufficiently large (140 eV) that differences between the two methods are insignificant, especially when considering other possible sources of error. In general, errors in extracting the single scattering distributions could arise from any uncertainty in the background extrapolation performed before the deconvolution. Also, the single scattering distributions will be less accurate for the thicker samples as triple and higher-order scattering events are more likely to fall outside the collection aperture. In our data, for cases where several thicknesses are available for a given deposition energy, we have noticed no significant errors resulting from the deconvolution procedure.

To characterize the normalized K-edge spectra, we have integrated the intensity over a small energy window of about 4 to 5 eV in width starting at the edge onset and extending to the intensity minimum between the π^* and σ^* peaks. This integral was then normalized by dividing by a similar integral from a standard spectrum recorded from graphitized evaporated carbon.[21] The resulting fraction, which we call f, is plotted in Fig. 2 as a function of deposition energy. This method for estimating f is essentially the same as that of Berger, McKenzie, and Martin,[18] but our integration window is slightly larger than theirs. Then our values of f, considered as measures of the π^* peak intensity, are very probably overestimated due to some contribution from the overlapping σ^* peak, but we chose such a window to obtain good statistical reproducibility. Each value of f shown in Fig. 2 represents an average over several spectra. The smallest values of f, presumably corresponding to the highest fraction of sp^3 hybridization, occur for deposition energies from about 50 to 600 eV.

There are additional aspects of the K-edge spectra which deserve mention. First, for those films deposited with ion-beam energies from 50 to 300 eV, there is a small shoulder which occurs just before the π^* feature as shown in Fig. 3. This has been observed by other investigators as well.[15] It has been attributed to core excitons or to dangling bonds but, at present, there is no completely satisfactory explanation for this feature. Second, the position of the π^* peak on the energy scale changes as its height decreases; for films with weak π^* peaks ($f \approx 0.2$), it shifts upward by about 0.4 eV compared to films with stronger π^* features such as those deposited at 10 eV where $f=0.86$. This shift is probably due to an overlap contribution from the nearby σ^* peak. Such an overlap is more significant as the π^* peak becomes weaker. Finally, we also note that the σ^* feature changes as a function of deposition energy. Within the deposition energy window of 50 to 600 eV, the integral of the σ^* feature is 10 to

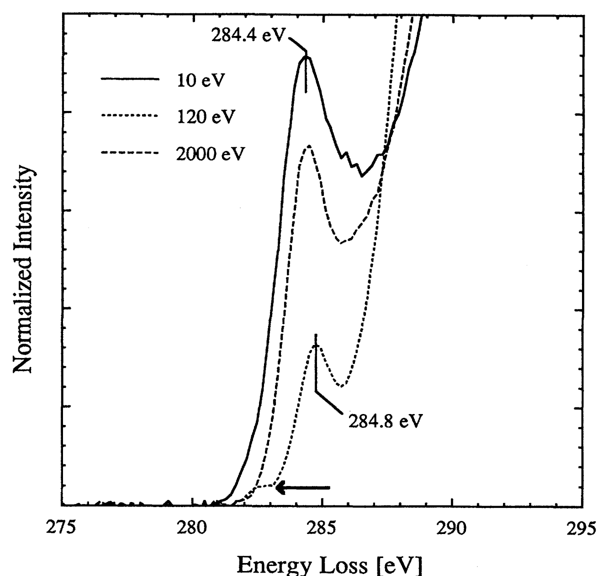

FIG. 3. Detail of the K-edge spectra from three films. The data from the 120 eV sample show that reduction of the π^* feature is accompanied by a small upward shift in energy of the peak by about 0.4 eV, the appearance of a small shoulder at about 282.5 eV, and an increase in the slope of the σ^* feature.

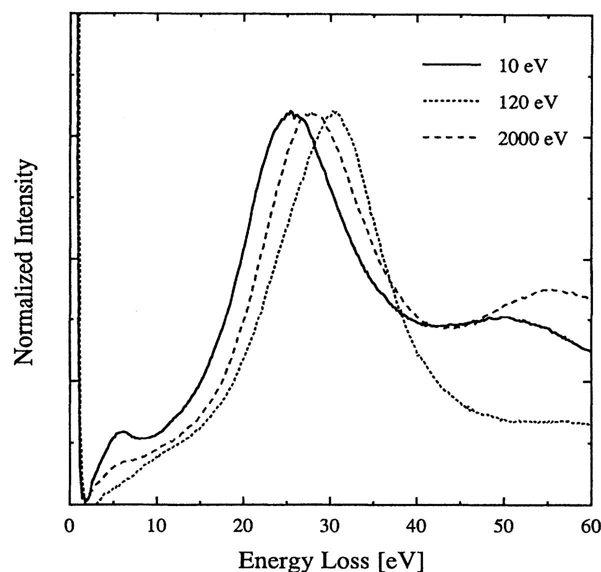

FIG. 4. Examples of low-loss spectra from three samples of MSIBD amorphous carbon. The 120 eV sample exhibits the highest energy for the plasmon resonance and also shows no sign of a π plasmon in the energy-loss region below 10 eV.

15 % higher than that observed in the samples prepared at 10 eV. The onset of this peak is also steeper.

Although there is no quantitative theory which predicts the strength of the π^* feature in EELS data from amorphous carbon, investigators have often taken it to be proportional to the number of sp^2-bonded atoms in the film.[15,18,19] We also assume that this is at least approximately true even though the details of the edge shape can be affected by such factors as the degree of short-range order. Furthermore, there is some overlap between the π^* and σ^* peaks making a clear separation of the two impractical, especially when the π^* peak is small. With these caveats, we nevertheless take f to be the fraction of sp^2-bonded atoms. Some investigators have made the additional assumption that the height of the σ^* peak is directly proportional to the number of σ-bonded electrons in the material and have used this assumption to normalize the spectra.[19] This means that only the relative heights of the π^* and σ^* features can be compared. We believe that the normalization procedure we have used allows us to compare the absolute heights of the π^* and σ^* features and not just their relative strengths. As noted above, we observed between a 10 and 15 % increase in the strength of the σ^* peak in a sample deposited with 120 eV ions as compared with one deposited with 10 eV. Based on the measured values of f, we should observe an increase of more than 20% if the integral of the σ^* peak is indeed directly proportional to the number of σ bonds in the material. This apparent discrepancy probably arises because it is not clear how to properly determine this integral. This is because a core electron ejected with, for example, 15 eV of energy in the direction of a π bond will contribute to the signal under the σ^* peak but does not really comprise part of the σ^* resonance signal. This contribution could be quite large for samples with high sp^2 content.

Low-loss spectra, recorded under the same conditions as the K-edge spectra, are shown in Fig. 4. The π plasmon at an energy loss of about 6.5 eV is entirely absent in the spectrum from the sample prepared with a 120 eV beam. At depositions of 2000 eV, the signal in this region is increased over that from the 120 eV sample but is still much less than that in the 10 eV sample. The main plasmon peak ranges from about 25 eV in the samples with the largest sp^2 content to as high as about 30 eV for the samples deposited with ion-beam energies between 50 and 600 eV. Figure 5 shows the correlation between the measured values of f and the plasmon energies for all the samples deposited at room temperature.

2. High temperature depositions

In a previous publication[21] we have presented energy-loss data from a sample deposited at a substrate temperature of 130 °C with a 120 eV ion beam. The data indicated a high degree of sp^3 bonding essentially identical to that of the ambient temperature depositions at the same ion beam energy. Among the present set of films examined is one deposited at 205 °C also with a 120 eV ion beam. The K-edge spectrum indicates that this film is essentially 100% sp^2 bonded. This result is in agreement with a previous study on the effect of substrate temperature for 120 eV depositions where it was found that a transition from high density (predominantly sp^3 bonded) to low density (sp^2 bonded) occurs at about 150 °C.[39] Also among the present set of films is one deposited at 165 °C with a 300 eV ion beam. For this film the K-edge spectrum is unaltered from that of the room-temperature samples. We conclude that for 300 eV depositions the substrate temperature required to suppress the formation of diamondlike films is greater than 165 °C.

The change in K-edge spectra as the films change from high density to low density with increasing substrate temperature is indicated in Fig. 6. Shown in the figure are spec-

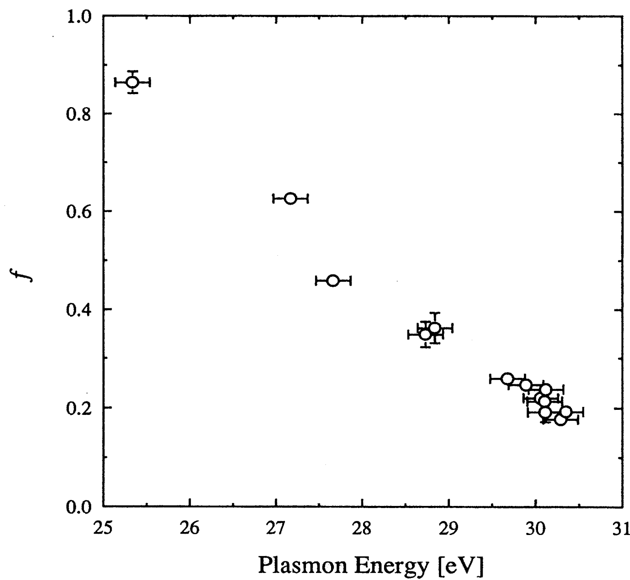

FIG. 5. Scatter plot of normalized π^* integrals vs bulk plasmon resonance energies for all room-temperature deposited films using ion beams ranging from 10 to 2000 eV.

tra from films deposited at 120 eV using substrate temperatures of 130 and 205 °C. Also shown is a spectrum from graphitized evaporated carbon for comparison. The spectrum from the film deposited at 205 °C exhibits some structure in the σ^* peak which is probably indicative of some degree of graphitic short-range order as it is similar to the spectrum from graphitized evaporated carbon. Also, the position of the π^* peak in this spectrum is at 285 eV, the same as that of graphitized evaporated carbon. This should be compared, for example, with the position of the π^* peak in the spectrum

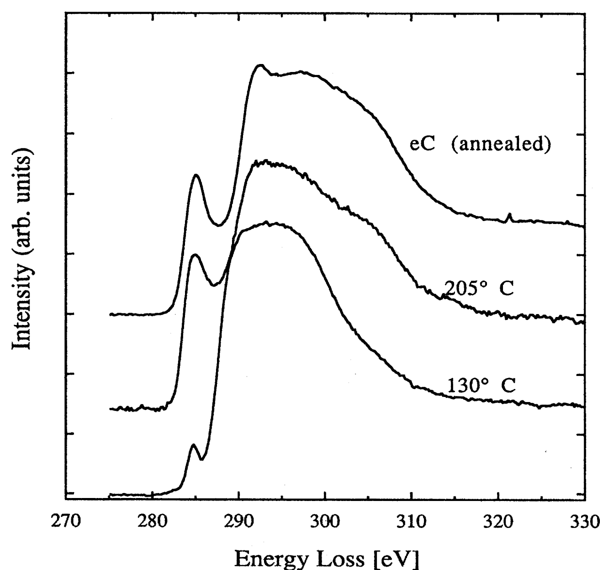

FIG. 6. K-edge spectra from samples deposited at 120 eV at temperatures of 130 and 205 °C. A spectrum from graphitized evaporated carbon is shown for comparison.

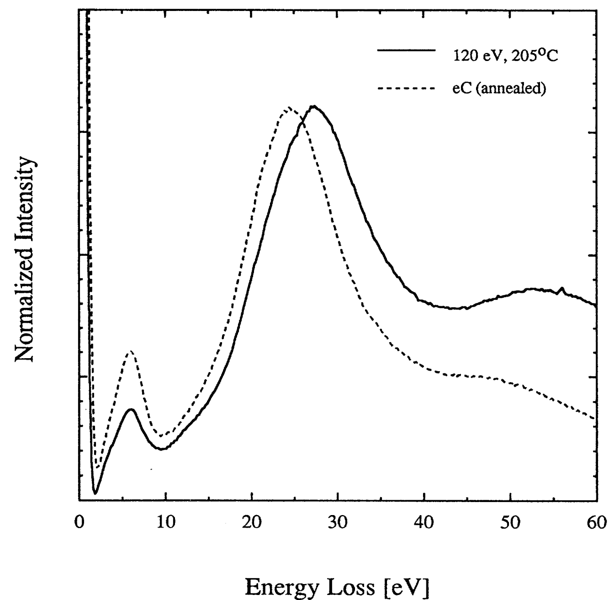

FIG. 7. Plasmon resonance in the sample deposited at 120 eV at 205 °C. A spectrum from graphitized evaporated carbon is also shown.

from the 10 eV room-temperature deposition where the sp^2 fraction is about 85% (cf. Figs. 2 and 3); the corresponding π^* peak is about 0.6 eV lower in energy. The shift upward to 285 eV is likely associated with graphitic short-range order.

Figure 7 shows the bulk plasmon resonances from the sample deposited at 205 °C using 120 eV ions and from the graphitized evaporated carbon (eC) sample. Both spectra exhibit pronounced π plasmon resonances, although that of the graphitized eC sample is stronger. (The spectra were normalized to the same height for the main plasmon resonances.) The main plasmon resonance for the MSIBD film is at a higher energy than that of the graphitized eC film: 26.9 eV as compared with 24.5 eV. This does not necessarily mean that the MSIBD film is denser than the eC film. In fact, we expect little difference in density if both are 100% sp^2 bonded. However, we note that graphite, despite having a density which is presumably similar to that of eC, has a plasmon resonance at 27 eV. This is due in part to the highly anisotropic nature of graphite. The plasmon resonance of 26.9 eV for the MISBD film in Fig. 7 is similar to that of graphite. High-resolution TEM and qualitative electron diffraction indicate that this particular film has a significant degree of short-range order. Although there is no evidence for crystallinity, on a scale of a few nanometers the film is anisotropic. This is particularly evident in high-resolution images from thin areas (where the film has presumably been torn) which reveal fringes (usually curved) with a spacing close to that of graphitic layers. We note that the eC sample must also have some degree of short-range graphitic order, so the reason that its resonance is not at the same energy is not clear. A quantitative comparison between the two samples of the degree of short-range order and of any possible preferred orientations for this order is necessary, and we have not, as yet, attempted any such comparison. However, one important point concerning this discrepancy is that the

eC is expected to be somewhat less dense than graphite simply because of voids and inefficient packing of atoms. This may explain, at least in part, the difference in plasmon resonances.

B. Quantitative diffraction

1. Standard data analysis

We have recorded filtered diffraction data from a number of the films deposited at room temperature and have attempted to determine the bond lengths in the films from these data. From the diffracted intensity one can obtain the reduced density function $G(r)=4\pi r[\rho(r)-\rho_0]$, where $\rho(r)$ is the average number density in $Å^{-3}$ at a distance r from an atom center and ρ_0 is the density averaged over the entire sample. The prescription for obtaining $G(r)$ from energy filtered electron diffraction has been summarized by Cockayne and McKenzie[24] and is analogous to that for x rays.[42] With $s=2(\sin\theta)/\lambda$, the desired expression is the following Fourier sine transform which we have indicated as a finite transform with an upper limit of s_m, the maximum value of s in the data scan:

$$G(r)=8\pi\int_0^{s_m} s\left[\frac{I(s)-Nf_C^2}{Nf_C^2}\right]D(s)\sin(2\pi sr)ds. \quad (1)$$

The quantity in brackets is the interference function. The quantity $I(s)$ is the intensity, f_C is the atomic scattering factor of a single carbon atom, and N is a normalization parameter which is typically determined by fitting the scattered intensity $I(s)$ to $Nf_C^2(s)$ at large s, that is, the interference function should oscillate weakly about zero at large s. For our scans s_m is usually between 3.5 and 4.0 $Å^{-1}$. We obtained f_C by fitting a cubic spline to the tabulated values of Doyle and Cowley.[43] The quantity $D(s)$ is a "modification" or "damping" function[24,44] often used to eliminate the spurious oscillations in the resulting reduced density function by reducing the contribution of the poorest (noisiest) data at higher s. We have used an exponential damping function $D(s)=\exp(-Bs^2)$, where B typically ranges between 0.2 and 0.3 depending on the statistics of the data. The use of this damping factor, however, will also broaden the peaks in $G(r)$ at low r.

Figure 8 shows the scattered intensity $I(s)$ for three films deposited at 10, 120, and 2000 eV. The data from the 120 eV sample are distinctly different from the scans obtained from the other films. The reduced density function $G(r)$ for the 120 eV sample is shown in Fig. 9. The positions and widths of the first four peaks agree well with those obtained by other investigators for similar films.[12–14,24,45]

2. Thickness corrections and scattering factor considerations

The behavior of $G(r)$ for small r in Fig. 9 is not the expected linear behavior; $G(r)$ at small r should be nearly equal to the straight line shown in the figure which is given by $-4\pi\rho_0 r$ with ρ_0 taken as 0.164, or 93% of the density of diamond. This estimate for the expected value of ρ_0 was obtained assuming a linear change in density as a function of sp^2 fraction f with $\rho_0=0.112$ $Å^{-3}$ (graphite) for $f=1$, and $\rho_0=0.176$ $Å^{-3}$ (diamond) for $f=0$. This kind of behavior in $G(r)$ for small r is usually indicative of a slow oscillation in the interference function.[46] One possibility is a poor choice of fitting parameter N, but we have been unable to eliminate the deep minimum at small r by varying N. Another possibility is multiple scattering. This would cause a redistribution of scattered intensity toward higher angles. Thus the measured intensity at large values of s would be higher than that for an ideal single scattering distribution. This would result in a larger fitted value for N, and the values of Nf_C^2 in the intermediate range of s would be too large as compared with a scattered intensity distribution which is already low in this range because of the redistribution of

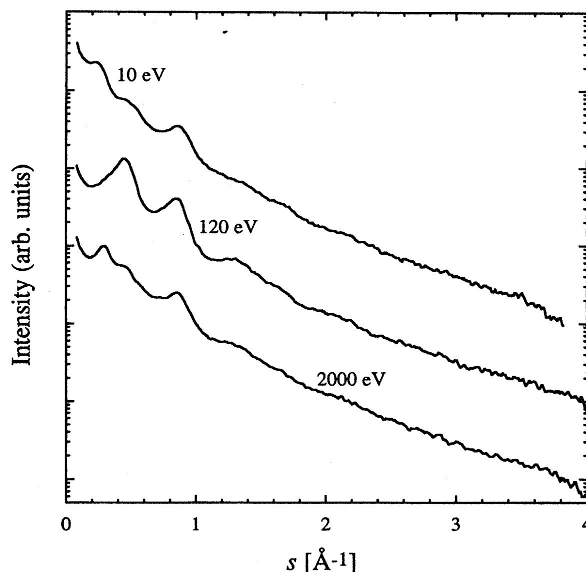

FIG. 8. Elastically scattered intensity (log scale) vs s for films deposited at 10, 120, and 2000 eV.

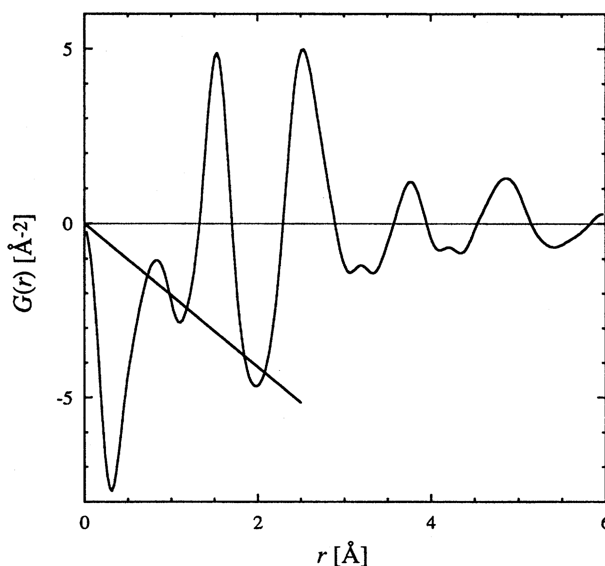

FIG. 9. Reduced density function $G(r)$ extracted from diffraction data from a film deposited at 120 eV. The expected linear behavior near the origin is indicated.

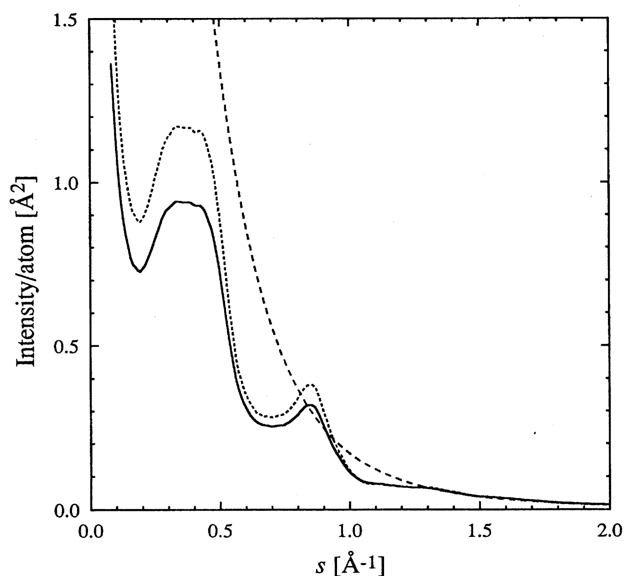

FIG. 10. Square of the scattering amplitude for a free carbon atom (dashed curve) shown with the measured scattered intensity divided by fitting parameter N for a film deposited at 30 eV (solid curve). The dotted curve shows the same data corrected for multiple scattering (assuming τ=0.3) and divided by an appropriate value of N.

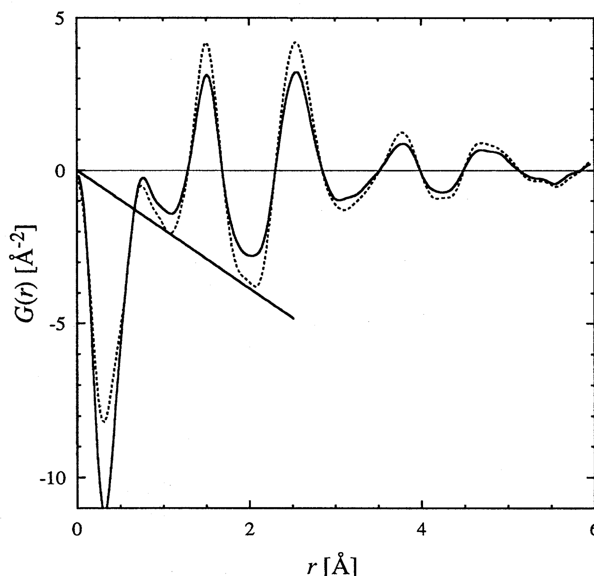

FIG. 11. Reduced density functions extracted from the raw data (solid curve) and deconvolved data (dotted curve) shown in Fig. 10. The expected linear behavior is indicated.

intensity to higher angles due to multiple scattering. For the particular sample used to generate the curve in Fig. 9, the thickness t was measured by profilometry to be t=460 Å. Under the assumption that the film is 93% as dense as diamond, we estimate that the mean free elastic scattering path Λ is ~2690 Å. The reduced thickness $\tau=t/\Lambda$ is then 0.17, so that, of the scattered intensity, about 8% is due to multiple scattering. (See the Appendix.)

Using a deconvolution procedure[47–49] (see the Appendix), we have attempted to account for multiple scattering in the data of Fig. 9 as well as data from thicker samples (~1000 Å) with τ perhaps as large as 0.3 or 0.4 where multiple scattering can account for between 15 to 20 % of the total scattered intensity. However, we were never able to obtain a reduced density function $G(r)$ which was well behaved near the origin. An example of the deconvolution results is shown in Figs. 10 and 11. Figure 10 is a plot of the atomic scattering intensity for a free carbon atom in units of Å^2 (dashed line) taken from Doyle and Cowley.[43] Also shown is the raw data and deconvolved data for a relatively thick carbon film (~1000 Å) deposited at 30 eV. The deconvolution was performed assuming a thickness of $\tau=t/\Lambda$=0.3. The data and the corrected data were each divided by an appropriate fitting parameter N to match the free atom scattering intensity at high angles. Despite the effective increased signal at low values of s in the corrected data, the reduced density function $G(r)$ shown in Fig. 11 is still poorly behaved near the origin, although it is somewhat improved in the sense that the minimum is no longer as deep. One can obtain further *apparent* improvement with the use of larger values for τ in the multiple scattering deconvolution; however, to use values much beyond τ=0.4 is physically unreasonable given the known thicknesses of these films. Finally, we note that the multiple scattering deconvolution procedure has a negligible effect on the extracted bond lengths. This agrees with the conclusions of Anstis, Liu, and Lake[49] based on computer-simulated data.

We suggest that the errors in this analysis are more fundamental than simple parameter misfits or uncorrected multiple scattering. Wright[44] has noted that for elements of low atomic number where a significant fraction of electrons are involved in bonding, x-ray data will yield correlation functions [such as $G(r)$] which are not well behaved below the first meaningful peak. The same must be true of electron diffraction from amorphous materials. Consequently, we believe that the nonlinear behavior of $G(r)$ near the origin arises due to our use of a single (free) atom scattering factor for carbon when, in fact, four of the six carbon electrons are involved in bonding resulting in an electron distribution which is significantly altered from that of a free carbon atom. We note that quantitative electron diffraction from amorphous carbon with a high fraction of sp^3 bonding has been reported in several publications by McKenzie and co-workers.[12–14,24,45] In all cases, $G(r)$ behaves similarly to our data or else is not shown by the authors for values of r less than about 0.5 Å. Also, in earlier filtered electron diffraction experiments on evaporated carbon similar difficulties were encountered; it was found necessary to alter the published values of the carbon scattering factor in an *ad hoc* fashion in order to force the linear behavior in $G(r)$ at small r.[50]

3. Results

With the caveat that extracted bond lengths may be slightly inaccurate due to the use of an incorrect scattering factor, we present the results for nine analyzed films. First- and second-neighbor bond lengths were obtained not from the function $G(r)$ but rather from the function $T(r)=G(r)+4\pi r\rho_0$. The value of ρ_0 had to be estimated

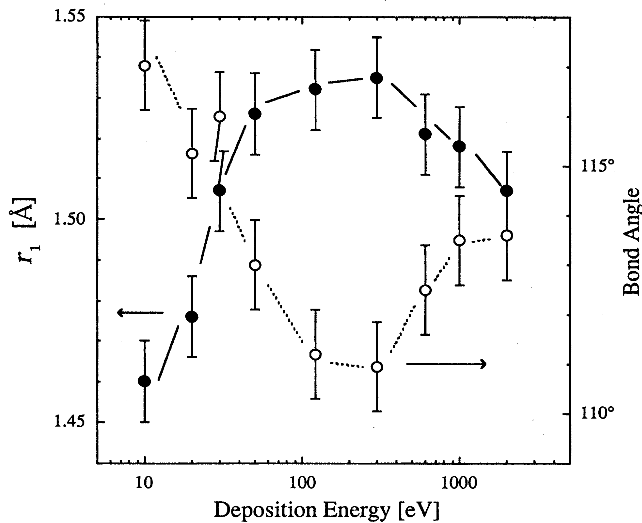

FIG. 12. Plots of nearest-neighbor distance r_1 (filled circles) and bond angle (open circles) vs deposition energy showing diamondlike structure between about 50 and 600 eV.

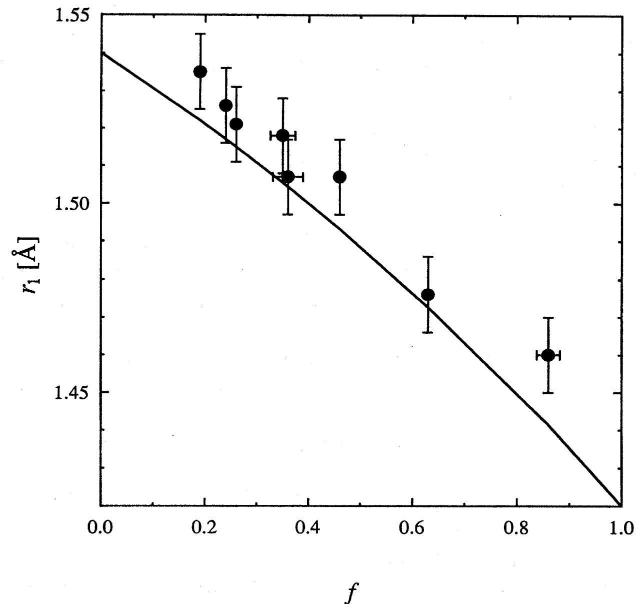

FIG. 13. Plot of nearest-neighbor distance r_1 vs sp^2 fraction. The curve shows the expected values based on a weighted average of graphitic and diamondlike bonding.

from other data, i.e., the K-edge spectra. However, inaccuracies due to these estimates are much less than the precision we quote for the bond lengths. Use of $T(r)$ as opposed to $G(r)$ for bond-length determination is preferable.[44] In our data, use of one or the other function has little effect on the first-neighbor bond length r_1, but the extracted second-neighbor distance r_2 can be almost 0.01 Å larger with the use of $T(r)$ rather than $G(r)$. The precision of the r_1 determinations is 0.01 Å. Figure 12 shows both r_1 and the bond angle θ vs deposition energy. Bond angles were determined from the relation $\theta = 2\sin^{-1}(r_2/2r_1)$. The bond length for the films deposited at 120 and 300 eV is 1.53 ± 0.01 Å. The measured bond angle is about $111\pm0.9°$. The bond length for diamond is 1.54 Å, and the true tetrahedral angle is 109.47°. The data are consistent with our interpretation of the K-edge spectra; between about 50 and 600 eV, the bond length is about 1.53 Å suggesting a high degree of sp^3 hybridization.

With regard to the accuracy of the bond-length measurements, we have already noted that use of an incorrect scattering factor may yield inaccurate results.[44] We have performed the same analysis on evaporated carbon, for which the expected bond length is that of graphite, 1.42 Å. We obtained a value of 1.44 ± 0.01 Å. The difference from the expected bond length suggests that this analysis does not yield highly accurate results possibly due to the incorrect scattering factor. It is certainly possible, however, that the bond length in amorphous evaporated carbon varies from that of graphite. Figure 13 is a plot of the measured bond lengths of various MSIBD films against the sp^2 fraction f as determined from K-edge spectra. The curve shown in the figure indicates the expected values of r_1 based on a weighted average of 1.42 and 1.54. That is, an sp^2-hybridized atom has three neighbors at a distance of $r_G=1.42$ Å, and an sp^3-hybridized atom has four neighbors at a distance of $r_D=1.54$ Å. The fraction f, of course, determines the hybridization fractions. The average nearest-neighbor distance is then

$$r_1 = \frac{3fr_G + 4(1-f)r_D}{4-f} . \quad (2)$$

The measured points all lie above the curve given by Eq. (2). If the curve is accurate, this result suggests that the structure analysis using the free atom scattering factor systematically overestimates the true nearest neighbor distance. Equation (2), however, is likely based on oversimplified assumptions. In particular, it assumes that a bond is not affected by its neighbors. Nevertheless, Eq. (2) is useful as an indication of the expected trend.

DISCUSSION

The purpose of the present work is to present the analysis of EELS data and diffraction data from MSIBD carbon films grown using a range of ion energies from 10 up to 2000 eV. Using spectral data from the carbon K edge together with reduced density functions extracted from quantitative diffraction analysis we have attempted to probe the atomic coordination of the carbon atoms in the interior of these noncrystalline films. The structural data lend further support to the interpretation of the spectral features at the K edge as being indicative of the relative amounts of trigonally and tetragonally coordinated carbon atoms. Taken together, the spectroscopy and the diffraction provide strong evidence for a substantial fraction of sp^3-bonded atoms for films grown within a rather broad energy window of about 50 to 600 eV. For energies less than about 30 eV, the films are predominantly sp^2 bonded. For energies above 600 eV, the sp^3 fraction decreases but remains at about 50% or higher. We have also determined the bulk plasmon energy for each film. Although this energy is not a direct measure of bulk density, for these isotropic amorphous films it can safely be taken as an indication of density changes, and, as such, correlates well with

the estimates of the sp^2 fraction determined from the K-edge spectra. High sp^2 fractions correspond to lower bulk plasmon resonance energies as would be expected for the lower density sp^2-bonded materials.

We interpret the data presented here in terms of the subplantation model originally proposed by Lifshitz and co-workers,[10] the basic features of which we summarize as follows: The implantation and growth process can be conveniently divided into three time scales. First, the major collisional processes occur on a time scale of roughly 10^{-13} s. These include stopping and incorporation of the impinging species in the subsurface layers of the film, atomic displacement events, backscattering, and sputtering. Second, on a time scale less than about 10^{-11} s, thermal relaxation occurs. This process, whereby the energy deposited by the energetic ion is dissipated, is somewhat poorly understood at present. Third, over times greater than about 10^{-10} s, long-term relaxation occurs. This includes the more conventional solid-state relaxation phenomena of diffusion, phase transformations, and chemical reactions.

When first proposing this model for film growth with hyperthermal species, Lifshitz and co-workers[10] presented supporting evidence in the form of Monte Carlo simulations as well as experimental evidence consisting of *in situ* surface analysis of growing films. An essential characteristic of the film growth which is clear from this evidence is that it is an internal process. The film grows by incorporation of impinging species into subsurface layers. Such growth is fundamentally different than that dominated by atoms captured at the surface, and recent experiments have served to emphasize the importance of internal growth in promoting the formation of dense films.[11,37,38] Such internal incorporation of impinging species is generally thought to lead to high internal stresses in the growing film; a number of authors have emphasized this aspect of the growth process. Several reports have included quantitative measurements of the residual stress present after completion of film growth,[12–15] and the concept has also served as a starting point for growth models.[16,17]

The subplantation model readily provides an explanation for the data presented here. For energies less than about 30 eV, few ions can penetrate the surface layers of the growing film. Growth is dominated by surface atoms as has been convincingly shown elsewhere.[11,37,38] The range between roughly 50 and 600 eV represents a near optimal window for the formation of dense diamondlike films. Penetration of the surface layers by the ions readily occurs allowing incorporation of additional atoms into the interior of the film resulting in internal growth. For energies greater than about 600 eV, it is the extended range and excessive collisional damage which become the important factors. Although the growth is still internal, with an increase in range there is a broader distribution and a subsequent smaller local density. Furthermore, atomic displacement damage should increase significantly as should sputtering yield, both serving to suppress the sp^3 fraction.

It is significant that the sp^3 fraction remains at or above about 50% for deposition energies as high as 2000 eV. This is in disagreement with data presented by other researchers.[12–15] Moreover, it highlights the poorly understood nature of the thermalization process. Davis[16] and Robertson[17] have independently proposed that in the higher-energy depositions rapid dissipation of the ion energy serves to severely repress the formation of the dense diamondlike phase. Our data indicate that this is not the case.

Regarding the data we have presented on a limited number of films grown at elevated substrate temperatures, we have seen that for 300 eV depositions at 165 °C the films retain a high sp^3 fraction. This result differs from the case of 120 eV depositions where it was shown by direct density measurements that the transition from diamondlike to low-density films occurs at about 150 °C.[38,39] The fact that substantial sp^3 fractions persist to higher substrate temperatures for the 300 eV depositions as compared with the 120 eV depositions is consistent with the subplantation model of the film growth. The growth of sp^2-bonded carbon results from the temperature-induced migration of implanted carbon towards the surface. As 300 eV ions have a greater penetration depth than 120 eV ions, the necessary migration paths are, on average, longer for the more energetic depositions. It thus requires a higher temperature to promote formation of sp^2-bonded carbon over sp^3-bonded carbon.

We note that the preferential growth of sp^2-bonded carbon with elevated temperature could become an important consideration if the ion-beam flux is sufficiently high. Arc systems, such as those used by some investigators,[12–15] are capable of deposition rates one to two orders of magnitude higher than our peak rate of 10^{16} atoms/s cm^2. If these high rates lead to a temperature increase, reduction of the sp^3 fraction in the film is a possibility.

Finally, we wish to emphasize a point concerning the bulk plasmon energies. The sample deposited with a 120 eV beam at a substrate temperature of 205 °C exhibited a plasmon resonance at about 27 eV. Despite what we believe to be 100% sp^2 bonding in the film, its plasmon resonance occurs at a higher energy than those of other films which have only 85% sp^2-bonded atoms and is in fact nearly equal to that of films with only 70% sp^2 bonding. We believe this result to be due to the locally anisotropic nature of that particular film. The value of 27 eV corresponds well with the bulk plasmon resonance energy of graphite. This result serves to emphasize that the plasmon energy is not a direct measure of density but can be sensitive to short-range order particularly when this order results in local anisotropy.

SUMMARY AND CONCLUSIONS

We have performed inelastic- and elastic-electron-scattering measurements in transmission geometry from MSIBD carbon films in order to probe the bonding states of the carbon atoms in the interior (bulk) of the films. Ion-beam energies used for deposition varied from 10 to 2000 eV.

Analysis of EELS data from the carbon K edge yields estimates of the fractions of sp^2- and sp^3-bonded atoms. For films grown with ion-beam energies less than 30 eV, the carbon atoms are predominantly sp^2 hybridized. The sp^3 fraction reaches its highest values (conservatively estimated at about 80%) within a broad window of deposition energies between 50 and 600 eV. The sp^3 fraction decreases with further increase in deposition energy but remains above 50% for energies as high as 2000 eV.

Bulk plasmon energies as a function of deposition energy

follow the same trend as the sp^3 fractions. Energies range from about 25.5 eV for the 10 eV deposition to about 30 eV for depositions between 50 and 600 eV. For the 2000 eV deposition, the plasmon energy drops down to 27.5 eV. The correlation of the plasmon resonance with the estimated sp^2 and sp^3 fractions indicates that the higher sp^3 fractions do in fact result in higher density material.

The elastic scattering data fully support the interpretation of the K-edge spectra. For the 10 eV deposition, the film with the highest sp^2 fraction, we measured a bond length of 1.46 Å and a bond angle of 117°. With increasing sp^3 fraction the bond length increases reaching a maximum of 1.53 Å while the bond angle decreases reaching a minimum of 111°. These values are close to those of diamond which are 1.54 Å and 109.47°.

ACKNOWLEDGMENTS

The authors would like to thank Professor S.C. Moss for many helpful discussions. This work was supported in part by the State of Texas through the Texas Center for Superconductivity, by the National Science Foundation under Grant No. DMR-9224377, and by the Israeli-US BSF Grant No. 92.

APPENDIX

In this appendix we discuss the occurrence of multiple scattering in electron diffraction from amorphous materials and describe the use of a deconvolution technique to remove its effects from the data. We make the assumption that there is cylindrical symmetry about the incident beam direction. If the scattering events can be taken as independent of each other, the intensity I_n, corresponding to scattering of order n and integrated over all angles, follows a Poisson distribution. For a sample of thickness t and with a mean free path for elastic scattering of Λ, the reduced thickness is $\tau = t/\Lambda$. With a primary beam of unit intensity, I_n is given by

$$I_n = \frac{\tau^n}{n!} \exp(-\tau). \tag{A1}$$

Consider the example mentioned in the text of a 460 Å thick film assumed to be 93% as dense as diamond. The mean free path for elastic scattering of 200 keV electrons in diamond is $\Lambda \approx 2500$ Å.[51] Then for the film $\Lambda \approx 2690$ Å. The reduced thickness is $\tau = t/\Lambda \approx 0.17$. From Eq. (A1) one calculates that, of the scattered intensity, about 8% is due to multiple scattering.

We now discuss a deconvolution technique to extract the single scattering distribution from the data. Mathematical details are given in the review paper by Scott.[48] The technique has also been described by Gjonnes,[47] and has been used on computer-generated data by Anstis, Liu, and Lake.[49] Primarily following the notation of Scott, we summarize the method. The assumption is made that the Ewald sphere can be approximated by its tangent plane. That is, all scattering distributions considered are strongly peaked in the forward direction. Given a cylindrically symmetric scattering distribution $F(s)$, which includes the unscattered portion of the primary beam, the Hankel transform, denoted $\tilde{F}(\xi)$, is

$$\tilde{F}(\xi) = 2\pi \int_0^\infty sF(s) J_0(2\pi s\xi)\, ds, \tag{A2}$$

where $J_0(x)$ is a Bessel function of the first kind of order 0 with argument x. Deconvolution depends on the fact that $\tilde{F}(\xi)$ can be written as[48]

$$\tilde{F}(\xi) = e^{\omega(\xi)t - \omega_0 t}, \tag{A3}$$

where $\omega(\xi)$ is the Hankel transform of the single scattering distribution $W(s)$, which is the quantity that we seek. The quantity t is the sample thickness, and $\omega_0 = \Lambda^{-1}$ where Λ is the mean free path for elastic scattering. Thus, assuming one has the complete scattering distribution $F(s)$ and one knows ω_0 and t, one can calculate the transform with Eq. (A2) and use Eq. (A3) to solve for $\omega(\xi)$. The inverse transform of $\omega(\xi)$ then yields the single scattering distribution $W(s)$. If only the product $\omega_0 t = t/\Lambda$ is known, one can still solve for $\omega(\xi)t$ which is sufficient.

Practical difficulties arise in determining t/Λ. In principle, the total integrated intensity I_t can be separated into two parts: $I_t = I_0 + I_s$, where I_0 is the unscattered portion and I_s the scattered part. The definition of the mean free elastic scattering path Λ is such that $I_0 = e^{-\tau} I_t$ where, as above, $\tau = t/\Lambda$ for thickness t. However, separation of scattered and unscattered components at $s=0$ is not possible. Furthermore, with our experimental arrangement we found it impractical to measure the intensity at $s=0$. Consequently, we do not have the complete scattering distribution. Even if the complete distribution were available, one would still have the difficulty of numerically calculating the integral of Eq. (A2) for a function F which is sharply peaked at the origin. One way around these difficulties is as follows. Assume the integral of $F(s)$ over s and the azimuthal angle to be normalized to unity. Approximate the unscattered beam as being proportional to a delta function at the origin. Let I_t be the intensity of the primary beam. Denote the scattered intensity as a function of s as $I'(s)$ to distinguish it from $I(s)$ which includes the unscattered portion. Then

$$I'(s) = I_t[F(s) - \delta(s)e^{-\tau}]. \tag{A4}$$

Denote the Hankel transform of $I'(s)$ as $\tilde{I}'(\xi)$. Using Eq. (A3) and taking the transform of the delta function as unity, one finds the transform of Eq. (A4) to be

$$\tilde{I}'(\xi) = e^{-\tau} I_t [e^{\omega(\xi)t} - 1]. \tag{A5}$$

Thus one can obtain a function proportional to the single scattering distribution $W(s)$ by taking the inverse transform of

$$\omega(\xi)t = \ln\left[\frac{\tilde{I}'(\xi)}{e^{-\tau} I_t} + 1\right]. \tag{A6}$$

This expression contains the transform of $I'(s)$ rather than the transform of the total distribution $I(s)$. The fact that in practice I' not only excludes the unscattered beam at the origin but also, in our case, may not be accurate near the origin is of no consequence for determining correlations at

the atomic scale. Also, the scattered intensity near the origin is a small portion of the total scattered intensity, so the accuracy of the deconvolution procedure is little affected.

It is still true that the quantity $I_0=I_t e^{-\tau}$ is unknown. The approach we took was to estimate I_s from the raw data and to treat τ as an adjustable parameter. With an estimate of I_s and a chosen value of τ, we obtain a value for $e^{-\tau}I_t=I_0=I_s/(e^{\tau}-1)$ which can be substituted in Eq. (A6).

[1] *Ion Bombardment Modification of Surfaces: Fundamentals and Applications*, edited by O. Auciello and R. Kelly (Elsevier, Amsterdam, 1987).

[2] *Thin Films from Free Atoms and Particles*, edited by K. J. Klabunde (Academic, Orlando, FL, 1985).

[3] *Plasma Deposited Thin Films*, edited by J. Mort and F. Jansen (CRC, Boca Raton, FL, 1986).

[4] R. A. Zuhr *et al.*, Nucl. Instrum. Methods Phys. Res. B **37-38**, 16 (1989).

[5] P. J. Martin, J. Mater. Sci. **21**, 1 (1986).

[6] S. M. Rossnagel and J. J. Cuomo, Vacuum **38**, 73 (1988).

[7] *Properties and Characterization of Amorphous Carbon Films*, edited by J. J. Pouch and S. A. Alterovitz (Trans. Tech, Aerdermannsdorf, 1990).

[8] D. Marton, in *Low Energy Ion-Surface Interactions*, edited by J. W. Rabalais (Wiley, London, 1994), p. 481.

[9] S. Aisenberg and R. Chabot, J. Appl. Phys. **42**, 2953 (1971).

[10] Y. Lifshitz, S. R. Kasi, and J. W. Rabalais, Phys. Rev. Lett. **62**, 1290 (1989); Y. Lifshitz *et al.*, Phys. Rev. B **41**, 10 468 (1990).

[11] Y. Lifshitz, G. D. Lempert, and E. Grossman, Phys. Rev. Lett. **72**, 2753 (1994).

[12] D. R. McKenzie *et al.*, Diamond Relat. Mater. **1**, 51 (1991).

[13] D. R. McKenzie *et al.*, Thin Solid Films **206**, 198 (1991).

[14] D. R. McKenzie, D. Muller, and B. A. Pailthorpe, Phys. Rev. Lett. **67**, 773 (1991).

[15] P. J. Fallon *et al.*, Phys. Rev. B **48**, 4777 (1993).

[16] C. A. Davis, Thin Solid Films **226**, 30 (1993).

[17] J. Robertson, Diamond Relat. Mater. **2**, 984 (1993); **3**, 361 (1994).

[18] S. D. Berger, D. R. McKenzie, and P. J. Martin, Philos. Mag. Lett. **57**, 285 (1988).

[19] J. J. Cuomo *et al.*, Appl. Phys. Lett. **58**, 466 (1991).

[20] K. W. R. Gilkes, P. H. Gaskell, and J. Yuan, Diamond Relat. Mater. **3**, 369 (1994).

[21] J. Kulik *et al.*, J. Appl. Phys. **76**, 5063 (1994).

[22] P. H. Gaskell *et al.*, Philos. Mag. B **66**, 155 (1992).

[23] K. W. R. Gilkes, P. H. Gaskell, J. Roberston, Phys. Rev. B **51**, 12 303 (1995).

[24] D. J. H. Cockayne and D. R. McKenzie, Acta Crystallogr. A Sect. **44**, 870 (1988).

[25] A. Saeed, P. H. Gaskell, and D. A. Jefferson, Philos. Mag. B **66**, 171 (1992).

[26] J. P. Hirvonen *et al.*, in *Properties and Characterization of Amorphous Carbon Films* (Ref. 7), p. 197.

[27] J. Ishikawa *et al.*, Nucl. Instrum. Methods Phys. Res. B **21**, 205 (1987).

[28] E. F. Chaikovskii, V. M. Puzikov, and A. V. Semenov, Sov. Phys. Crystallogr. **26**, 122 (1981).

[29] J. H. Freeman, W. Temple, and G. A. Gard, Vacuum **34**, 305 (1984).

[30] R. S. Nelson *et al.*, Proc. R. Soc. London Ser. A **386**, 211 (1983).

[31] T. Miyazawa *et al.*, J. Appl. Phys. **55**, 188 (1984).

[32] S. R. Kasi, H. Kang, and J. W. Rabalais, J. Chem. Phys. **88**, 5914 (1988).

[33] W. M. Lau *et al.*, J. Appl. Phys. **70**, 5623 (1991).

[34] Y. Lifshitz, S. R. Kasi, and J. W. Rabalais, in *Properties and Characterization of Amorphous Carbon Films* (Ref. 7), p. 237.

[35] See, e.g., R. Brydson, Bull. Electron Microsc. Soc. Am. **21**, 57 (1991), and references therein.

[36] Y. Lifshitz *et al.*, Diamond Relat. Mater. **3**, 542 (1994).

[37] E. Grossman *et al.*, Appl. Phys. Lett. (to be published).

[38] Y. Lifshitz *et al.*, Diamond Relat. Mater. **4**, 318 (1995).

[39] Y. Lifshitz *et al.*, Diamond Relat. Mater. **2**, 285 (1993).

[40] R. F. Egerton, *Electron Energy-Loss Spectroscopy in the Electron Microscope* (Plenum, New York, 1986).

[41] R. F. Egerton, Y.-Y. Yang, and S. C. Cheng, Ultramicroscopy **48**, 239 (1993).

[42] See, e.g., B. E. Warren, *X-ray Diffraction* (Addison-Wesley, Reading, MA, 1969); A. Guinier, *X-ray Diffraction in Crystals, Imperfect Crystals, and Amorphous Bodies* (Freeman, San Francisco, 1963); H. P. Klug and L. E. Alexander, *X-ray Diffraction Procedures for Polycrystalline and Amorphous Materials* (Wiley, New York, 1954).

[43] P. A. Doyle and J. M. Cowley, in *International Tables of Crystallography*, edited by J. A. Ibers and W. C. Hamilton (Kynock, Birmingham, England, 1974), Vol. IV, p. 152.

[44] A. C. Wright, J. NonCryst. Solids **106**, 1 (1988).

[45] D. A. Muller, in *Proceedings of the 51st Annual Meeting of the Microscopy Society of America*, edited by G. W. Bailey and C. L. Rieder (San Francisco Press, San Francisco, 1993), p. 1100.

[46] R. Kaplow, S. L. Strong, and B. L. Averbach, Phys. Rev. **138**, A1336 (1965).

[47] J. Gjonnes, Acta Crystallogr. **12**, 976 (1959).

[48] W. T. Scott, Rev. Mod. Phys. **35**, 231 (1963).

[49] G. R. Anstis, Z. Liu, and M. Lake, Ultramicroscopy **26**, 65 (1988).

[50] J. F. Graczyk, Ph.D. thesis, Massachusetts Institute of Technology, 1968.

[51] L. Reimer and K. H. Sommer, Z. Naturforsch. **23a**, 1569 (1968).